Explaining Cold-Pulse Dynamics in Tokamak Plasmas Using Local Turbulent Transport Models

P. Rodriguez-Fernandez, A. E. White, N. T. Howard, B. A. Grierson, G. M. Staebler, J. E. Rice, X. Yuan, N. M. Cao, A. J. Creely, M. J. Greenwald, A. E. Hubbard, J. W. Hughes, J. H. Irby, and F. Sciortino

Explaining Cold-Pulse Dynamics in Tokamak Plasmas using Local Turbulent Transport Models

P. Rodriguez-Fernandez,[1] A.E. White,[1] N.T. Howard,[1] B.A. Grierson,[2] G.M. Staebler,[3] J.E. Rice,[1] X. Yuan,[2] N.M. Cao,[1] A.J. Creely,[1] M.J. Greenwald,[1] A.E. Hubbard,[1] J.W. Hughes,[1] J.H. Irby,[1] F. Sciortino[1]

[1] *MIT Plasma Science and Fusion Center, Cambridge, Massachusetts 02139, USA*
[2] *Princeton Plasma Physics Laboratory, Princeton, New Jersey 08540, USA*
[3] *General Atomics, P.O. Box 85608, San Diego, California 92186-5608, USA*

A long standing enigma in plasma transport has been resolved by modeling of cold-pulse experiments conducted on the Alcator C-Mod tokamak. Controlled edge cooling of fusion plasmas triggers core electron heating on timescales faster than an energy confinement time, which has long been interpreted as strong evidence of non-local transport. This work shows that the steady state profiles, the cold-pulse rise time and disappearance at higher density as measured in these experiments are successfully captured by a recent local quasilinear turbulent transport model, demonstrating that the existence of non-local transport phenomena is not necessary for explaining the behavior and timescales of cold-pulse experiments in tokamak plasmas.

For twenty years, an enigmatic but universal transient transport phenomenon in fusion plasmas has challenged the standard local model of transport: an increase of core temperature associated with edge cooling on timescales faster than the energy confinement time [1, 2]. These perturbative transport effects have been interpreted as non-local phenomena, requiring explanation outside of the standard local-transport paradigm [2]. Cold-pulses have been conducted on both tokamaks and stellarators (TEXT [3], TFTR [4], Tore Supra [5], RTP [6], ASDEX Upgrade [7], JET [8], LHD [9], HL-2A [10], Alcator C-Mod [11] and KSTAR [12]). In these experiments, a sharp drop in edge electron temperature results from the deposition of neutral particles at the periphery of the plasma, usually via laser ablation. A rapid response (faster than an energy confinement time [13]) of the core temperature is observed. Interestingly, these core temperature increases in response to the edge cooling do not appear in high-density plasmas [14]. Because the behavior is observed ubiquitously, it has emerged as the most well-known example of "non-local" transport in fusion plasmas [1, 2]. As such, this observation has called into question the well-established picture of core turbulent transport based on electromagnetic drift-wave type turbulence driven by local pressure gradients [15, 16]. Because no single standard local transport model tried to date has been able to reproduce satisfactorily all the observed temporal behavior in the experiments [7, 8, 17], these transient transport phenomena feature prominently as an open question in review articles on non-local transport [2] and as a challenge for predictive capabilities in tokamak burning plasmas, as discussed in the ITER transport physics basis paper [18].

This Letter demonstrates that cold-pulse phenomena in tokamak plasmas can be fully explained by local transport models, including the disappearance of the core temperature inversions at high density. While truly non-local effects may be present in stellarators [2], we focus on cold-pulse behavior in tokamaks. The quasilinear transport

models considered are widely applied for predictions of equilibrium pressure profiles [19, 20]. Specifically, we use the recently developed trapped gyro-landau fluid model TGLF, which contains a rule for the turbulence saturation (TGLF-SAT1) where the zonal flow mixing, rather than shearing, is the primary saturation mechanism of both ion and electron scale turbulence [21, 22]. The new saturation rule came about as a consequence of cross-scale coupling physics, first identified in high-fidelity, realistic mass ratio multiscale nonlinear gyrokinetic simulations [23]. The original saturation rule (TGLF-SAT0) [24] does not include cross-scale coupling . TGLF-SAT1 gives a larger amplitude to intermediate-k modes than in TGLF-SAT0, and is also able to capture the nonlinear upshift (Dimits shift) of the critical ion temperature gradient at low-k [22]. Furthermore, experimental electron temperature profile stiffness is underpredicted with TGLF-SAT0, but can be matched by the higher stiffness TGLF-SAT1 model [25].

By comparing the new saturation model, TGLF-SAT1, to the original model, TGLF-SAT0, we are able to identify that the physical origin of cold-pulse dynamics is a competition between density gradient driven trapped electron mode (TEM) turbulence and ion temperature gradient (ITG) driven turbulence. Interestingly, TGLF-SAT1 simulations with only ion scale turbulence, $k_\theta \rho_s \sim O(1.0)$, can reproduce experiment as well as simulations that include multi-scale turbulence, $k_\theta \rho_e \sim O(1.0)$. Here, k_θ is the poloidal wavenumber, ρ_e is the electron gyroradius, and ρ_s is the ion gyroradius evaluated with the ion sound speed ($c_s = \sqrt{T_e/m_i}$). This indicates that multi-scale interactions and cross-scale energy transport recently discovered in nonlinear gyrokinetic simulations [23, 26] play a subdominant role in determining the cold-pulse dynamics in these experiments.

Here we describe modeling of one dedicated experiment at Alcator C-Mod [11], which exhibits the cold-pulse phenomena observed ubiquitously in fusion plasmas. Cold-pulses are introduced at the edge of an Ohmic
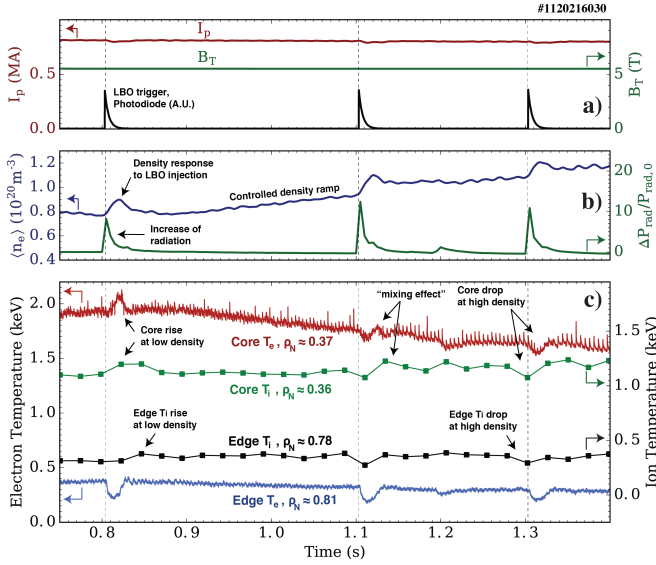
FIG. 1. Experimental parameters. (a) Plasma current, toroidal field and LBO injection times; (b) line-averaged density and total radiated power normalized to pre-cold pulses time; (c) core and edge electron and ion temperatures. Details on diagnostic systems can be found in Refs. [11, 27].
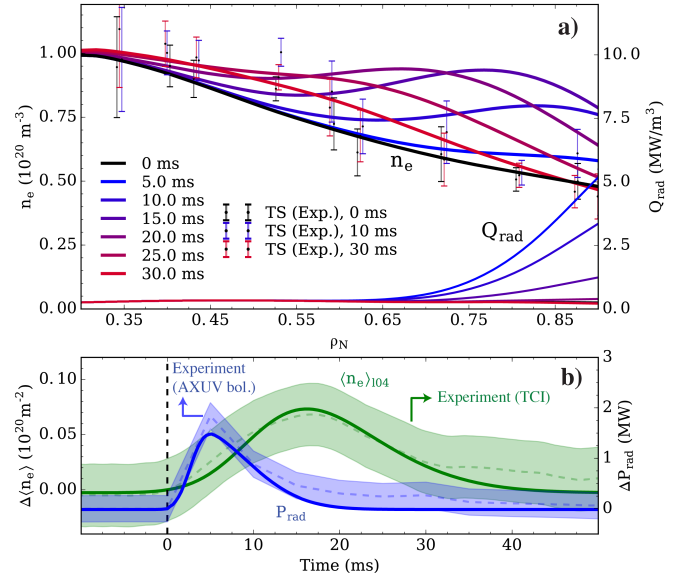

FIG. 2. Low-density plasma. (a) Density perturbation and radiative sink introduced to model cold-pulse injection. (b) Simulated and experimental changes in line-integrated density (error bar calculated from low frequency subtraction errors) and total radiated power (error bar estimated from Ref. [30]).

L-mode plasma ($B_T = 5.5T$, $I_p = 0.8MA$) via injection of CaF_2 impurities using a laser blow-off system [28] during a controlled density ramp, as shown in Figs. 1a and 1b. At high density, this discharge transitions from LOC (Linear Ohmic Confinement regime) to SOC (Saturated Ohmic Confinement regime), concomitant with a change in intrinsic rotation direction. Line-averaged density and total radiated power (Fig. 1b), electron temperature, T_e, and ion temperature, T_i, (Fig. 1c) are perturbed by the impurity injection. Past work showed that the size of the edge perturbation does not affect the core temperature inversion in Alcator C-Mod [29]. At this plasma current, the controlled density ramp covers the transition from "non-local" to "standard" transport behavior (disappearance of temperature inversion) in both electron and ion channels, as shown in Fig. 1c. Core inversions of T_e and T_i, as well as an edge T_i inversion, are only observed in the low-density portion of the discharge.

In the simulations, implicit transport equations are solved using the PT_SOLVER numerical scheme integrated with the TRANSP power balance code [31]. The transport model consists of both neoclassical (Chang-Hinton model) and turbulent transport (TGLF model). The experimental ion and electron temperatures at radial position $\rho_N = 0.9$ (square root of the normalized toroidal flux), taken prior to the cold-pulse injection, are used as boundary conditions for the transport model. Ion and electron temperature profiles are self-consistently evolved in time until reaching a steady state, while density is held fixed. In these simulations, current diffusion is not self-consistently modeled, and total plasma current and applied magnetic field are kept constant in time. It has been

previously demonstrated in experiments that changes in the magnetic equilibrium do not affect the core temperature response [3, 8]. Additionally, current diffusion is much slower than the observed onset of the temperature inversion. Recent work [29] showed no changes in the core response during intrinsic rotation reversals, suggesting that coupling between momentum and heat transport may not play a role in the phenomenology of temperature inversions. Therefore, plasma intrinsic rotation is not evolved in the simulations. In order to avoid any interactions with sawtooth activity [5], the analysis of the results is restricted to the region outside the sawtooth inversion radius, $\rho_N > 0.3$.

Once the steady-state temperature profiles are obtained, we introduce a time-evolving cold-pulse in the simulation by accounting for two major effects observed in the experiment: enhanced radiation losses and impurity density perturbation. Both effects are introduced as inputs with skewed-Gaussian shapes in space and time (Fig. 2a), using the experimental constraints of the measured total radiated power and line-averaged density, as shown in Fig. 2b. The radiative sink is localized at the periphery of the plasma (peaked at $\rho_N \simeq 0.95$), in order to reproduce the experimentally measured increase in total radiated power. The impurity density evolution is modeled as an inwardly propagating skewed-Gaussian, by self-consistently varying Z_{eff} and electron density profiles, such that main ion density remains constant during the injection. This technique for introducing the cold-pulse in the simulation is used because the onset of the electron and ion temperature perturbations can be modeled self-consistently. This is a critical difference with
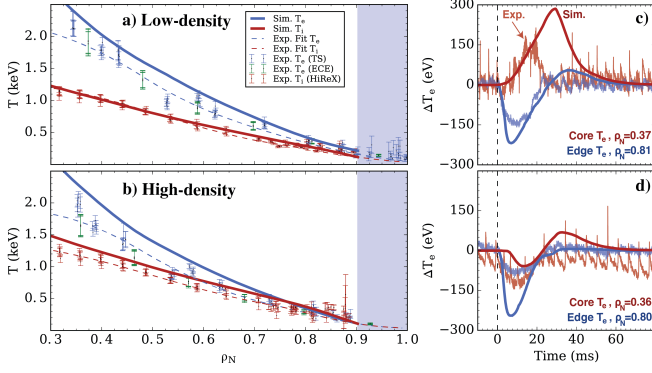
FIG. 3. Steady-state ion and electron temperature profiles in experiment and simulation (TGLF-SAT1 high-k) for (a) low-density and (b) high-density. Evolution of edge and core electron temperature after cold-pulse injection for (c) low-density and (d) high-density.

past work using quasilinear models [7, 17], in which the edge temperatures were often manually adjusted outside of experimentally relevant ranges to produce the desired amplitude of the core temperature inversion. Figs. 3a and 3b show simulated electron and ion temperatures in steady-state at low and high density, $\langle n_e \rangle \simeq 0.8 \cdot 10^{20} m^{-3}$ and $\langle n_e \rangle \simeq 1.1 \cdot 10^{20} m^{-3}$, respectively. In this simulation, turbulent transport is modeled using TGLF-SAT1, with a standard $k_\theta \rho_s$-grid to account for contributions up to $k_\theta \rho_s = 24.0$ ("high-k"). At the position of interest, $\rho_N \approx 0.36$, both electron and ion temperature steady-state profiles are within two-sigma experimental error bars.

First, we investigate the low-density condition, where the core temperature inversion is observed experimentally, by comparing the simulated transient behavior of the electron temperature after the cold-pulse injection to the experiment, using TGLF-SAT1 high-k (Fig. 3c). To be conservative, we define an onset time for the core temperature (in both the simulation and the experiment) to be the time at which the mean value has increased by more than one experimental standard deviation ($27eV$). The experimental onset time is $7ms$, and the experimental energy confinement time is $22ms$. In the simulation, the onset time is calculated to be $7ms$, and the energy confinement time is $39ms$. Hence, the simulation captures the prompt response (faster than energy confinement time) of the core temperature to the edge perturbation. Past work [17] using several quasilinear transport models, including GLF23 [32] the predecessor to TGLF, was unable to create core temperature inversions of high enough magnitude to match the observed peak temperature. In our case, predictions for the core temperature evolution reach the experimental peak value at $16ms$, and continue to rise higher than the peak experimental value. Because the background equilibrium predicted by the simulation (see Fig. 3a) is at a lower collisionality due to the overpredicted electron temperature for fixed density, it causes the simulated inversion to achieve higher

peak values before decay, and to last longer, consistent with experimental trends [29]. The edge temperature drop is overpredicted, outside error bars, in the simulations. We have run cases in which the modeled edge drop and core inversion are forced to match the experiment. In these cases, the density perturbation and the radiated power are inconsistent with the experimental measurements. Simulations with TGLF-SAT1 run only up to $k_\theta \rho_s \leq 3.0$ ("low-k") could also capture the experimental behavior, whereas TGLF-SAT0 strongly overpredicted the steady-state electron and ion temperatures outside two-sigma experimental error bars, as well as the onset time of the core response ($14ms$), which reached a smaller peak amplitude. In addition to the higher stiffness and critical gradient, the new saturation rule in TGLF-SAT1 gives a larger amplitude to intermediate-k modes than in TGLF-SAT0, which likely enhances the impact of the TEM on the fluxes.

In order to interpret these results and understand the origin of the cold-pulse phenomena, we consider the changes in electron and ion transport and subsequent changes in the power balance terms in the TGLF-SAT1 high-k simulation. Collisional equilibration comes into play as a source or sink of stored energy for ions and electrons, but our modeling shows that it is not the dominant contribution in the low collisionality plasmas where the core temperature inversions appear. This is one of the main differences with respect to past integrated modeling approaches [7, 8, 17], where the collisional equilibration was a dominant mechanism in creating an inversion. Instead, our results show that core turbulence stabilization due to a reduction of the driving gradients plays the dominant role. Given that heat fluxes may depend on electron temperature (a/L_{T_e}), ion temperature (a/L_{T_i}) and density (a/L_n) gradients, the three channels are coupled via turbulence stabilization. Fig. 4a duplicates Fig. 3c, with dashed lines indicating time points of interest, and Fig. 4b shows the time evolution of edge and core ion temperature. Figs. 4c and 4d depict the evolution of the core gradients and their effect on the total conducted power profile, respectively. Drops in both a/L_n and a/L_{T_i} stabilize turbulence and therefore reduce the conducted power losses. Such a drop in the conducted power leads to a transient increase in the stored energy, as shown in Fig. 4e. The time-derivative of the electron stored energy, $\frac{\delta W}{dt}$, traces the opposite evolution to the conducted power density, ∇q_e, which means that changes in transport dominate the time behavior. This interplay between channels depends on the turbulence at each radial position during the propagation of the cold-pulse. Fig. 4f depicts the reduction of the growth rates of the most unstable mode at the core of the plasma following the cold-pulse arrival. In this case, the plasma core is observed to be dominated by density gradient driven trapped electron modes, which are stabilized by the a/L_n reduction. It is worth pointing out that the onset time of core T_e, although faster than the energy confinement time, is slow compared to the turbulence decorrelation
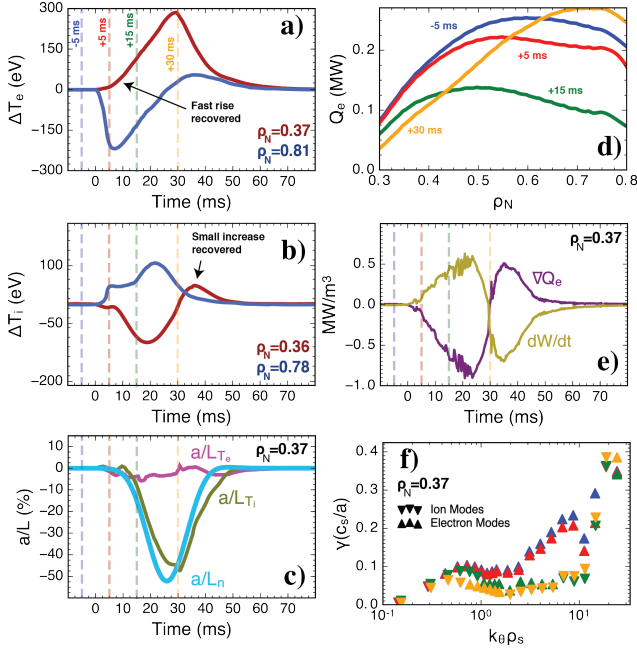
FIG. 4. Simulation results at low-density. (a) Edge and core electron temperature; (b) Edge and core ion temperature; (c) Normalized gradient scale lengths; (d) Volume-integrated electron heat flux at different times after the injection; (e) Conducted electron power density and rate of increase of stored energy; (f) Growth rates of most unstable mode.
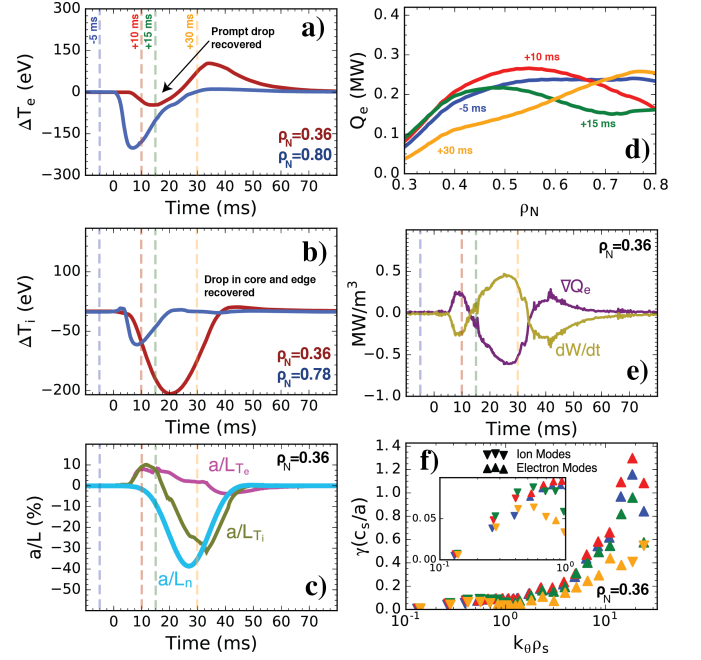

FIG. 5. Simulation results at high-density. (a) Edge and core electron temperature; (b) Edge and core ion temperature; (c) Normalized gradient scale lengths; (d) Volume-integrated electron heat flux at different times after the injection; (e) Conducted electron power density and rate of increase of stored energy; (f) Growth rates of most unstable mode.

time, estimated as $1/\gamma_{low-k} \sim 6.5 \mu s$ from TGLF at the low-k maximum ($k_\theta \rho_s \sim 0.7$). We note that this peak is consistent with strong TEM activity.

Simulated ion response is also qualitatively consistent with experimental observations here and previously at C-Mod [27]. The simulations recover a small, late increase in the core T_i (Fig. 4b), as well as an increase in T_i at the edge, which arises due to the stabilization of turbulence. In contrast to the electron temperature, which is measured in the experiment with a time resolution of $0.05 ms$, the time resolution of the measured ion temperature was $24 ms$, making it challenging to perform direct comparison of timing of core and edge ion temperature rises. This work, however, does show that a large core ion temperature increase is not needed to recover the electron temperature inversion, contrary to past modeling work [17] and consistent with the fact that a temperature increase in the electron channel is observed in other experiments regardless of the ion response [7, 33]. Unlike the TGLF-SAT1 simulations, TGLF-SAT0 did not recover an ion temperature increase at the plasma core.

Having shown that we capture the cold-pulse dynamics at low density, next we test the model for high density (Fig. 3d). In the experimental discharge, the density was increased by 37%, and a second cold-pulse was injected, which leads to the standard core temperature decrease (Fig. 1c). Figs. 5a and 5b show the simulation time histories of electron and ion temperature, respectively, with times of interest marked again by dashed lines. The sim-

ulated drop in the core (red trace) in Fig. 5a is lower than the experimental core drop (Fig. 3d), outside of error bars. The minimum core temperature occurs $14 ms$ after the injection in the simulation, and $10 ms$ in the experiment. The simulated drop in the edge (blue trace) in Fig. 5a is larger than the experimental drop. The minimum edge temperature occurs $7 ms$ after the injection in the simulation, and $10 ms$ in the experiment. Hence, the simulation at high-density does not capture quantitatively the experimental magnitudes and time-scales. It does, however, reproduce qualitatively the disappearance of the prompt core temperature increase, as well as the ion temperature drop. A later electron temperature rise is observed in the simulation (peak at $35 ms$), not present in the experiment. This feature can be explained, again, by the underprediction of collisionality. Given the trends found in past work [29], the plasma at the simulated collisionality approaches the "transition regime" and therefore a "mixing effect" (drop followed by a rise) is present. We have run simulations at higher density, past the transition regime, and no temperature increase is observed.

At higher density, the disappearance of temperature inversions, in both the ion and the electron channels, Figs. 5a and 5b, respectively, is attributable to a stronger effect of the ion temperature gradient scale length on electron and ion heat transport, characteristic of SOC plasmas [34]. Furthermore, the higher edge collisional coupling causes the edge ion temperature to drop along

with the electron temperature, causing the propagation of an ion cold-pulse and subsequent increase in a/L_{T_i}, as shown in Fig. 5c. As depicted in Fig. 5f, low-k ion modes are destabilized on a fast time-scale and the conducted heat flux is increased (Fig. 5d), causing the fast reduction of electron stored energy (Fig. 5e). Past experimental work suggested that the disappearance of temperature inversions could be connected to the TEM/ITG paradigm [11], which is consistent with the results presented here.

Past results [7, 8, 17] with different quasilinear models were unable to achieve the level of agreement with all the experimentally observed cold-pulse phenomena that is now achieved with TGLF-SAT1. For this reason, cold-pulse propagation had been considered a primary example of the existence of non-local transport effects, not encapsulated in the local transport paradigm [2]. In this work, we have shown that the recently developed trapped gyro-landau fluid model TGLF-SAT1 [21, 22] includes the key physics required to reproduce the experimental cold-pulse dynamics in tokamaks. By examining the results from TGLF-SAT1 high-k simulations, we find that the cold-pulse phenomena can be explained by the competition between density gradient driven TEM and ITG turbulence. By comparing among TGLF-SAT1 high-k, TGLF-SAT1 low-k and TGLF-SAT0 high-k simulations, we find that cross-scale coupling is less important than capturing the nonlinear upshift of the critical gradient, the profile stiffness, and the enhanced TEM activity when predicting dynamical cold-pulse behavior. The TGLF-SAT1 model is able to quantitatively capture the prompt onset of the core T_e inversion. Furthermore, the magnitude is qualitatively consistent with experimental trends, and the disappearance at high-density is observed. The model also qualitatively reproduces the edge and core ion temperature increases at low density and decreases at high density. To the authors' knowledge, these results provide the strongest evidence to date that the cold-pulse phenomena in tokamaks can be captured by the standard paradigm of local transport, without the need to invoke non-local transport effects. By means of experimentally-constrained self-consistent modeling of cold-pulse experiments, we have shown that the existence of non-local transport phenomena is not necessary for explaining the behavior and timescales of cold-pulse experiments in tokamak plasmas.

[1] J. D. Callen and M. W. Kissick, Plasma Phys. Control. Fusion **39**, B173 (1997).
[2] K. Ida *et al.*, Nucl. Fusion **55**, 013022 (2015).
[3] K. W. Gentle *et al.*, Phys. Rev. Lett. **74**, 3620 (1995).
[4] M. Kissick *et al.*, Nucl. Fusion **36**, 1691 (1996).
[5] T. Dudok de Wit *et al.*, Phys. Plasmas **5**, 1360 (1998).
[6] P. Mantica *et al.*, Phys. Rev. Lett. **82**, 5048 (1999).
[7] F. Ryter *et al.*, Nucl. Fusion **40**, 1917 (2000).
[8] P. Mantica *et al.*, Plasma Phys. Control. Fusion **44**, 2185 (2002).
[9] S. Inagaki *et al.*, Phys. Rev. Lett. **107**, 115001 (2011).
[10] X. Duan *et al.*, Nucl. Fusion **49**, 104012 (2009).
[11] J. Rice *et al.*, Nucl. Fusion **53**, 033004 (2013).
[12] Y. Shi *et al.*, Nucl. Fusion **57**, 066040 (2017).
[13] J. G. Cordey *et al.*, Plasma Phys. Control. Fusion **36**, A267 (1994).
[14] M. Kissick *et al.*, Nucl. Fusion **38**, 821 (1998).
[15] A. J. Brizard and T. S. Hahm, Rev. Mod. Phys. **79**, 421 (2007).
[16] X. Garbet *et al.*, Nucl. Fusion **50**, 043002 (2010).
[17] J. E. Kinsey *et al.*, Phys. Plasmas **5**, 3974 (1998).
[18] E. Doyle *et al.*, Nucl. Fusion **47**, S18 (2007).
[19] R. Budny *et al.*, Nucl. Fusion **56**, 056002 (2016).
[20] H.-T. Kim *et al.*, Nucl. Fusion **57**, 066032 (2017).
[21] G. M. Staebler *et al.*, Phys. Plasmas **23**, 062518 (2016).
[22] G. Staebler *et al.*, Nuclear Fusion **57**, 066046 (2017).
[23] N. Howard *et al.*, Nucl. Fusion **56**, 014004 (2016).
[24] G. M. Staebler *et al.*, Phys. Plasmas **14**, 055909 (2007).
[25] P. Rodriguez-Fernandez *et al.*, Fusion Technol. (to be published).
[26] S. Maeyama *et al.*, Nucl. Fusion **57**, 066036 (2017).
[27] C. Gao *et al.*, Nucl. Fusion **54**, 083025 (2014).
[28] N. T. Howard *et al.*, Rev. Sci. Instrum **82** (2011).
[29] P. Rodriguez-Fernandez *et al.*, Nucl. Fusion **57**, 074001 (2017).
[30] R. L. Boivin *et al.*, Rev. Sci. Instrum **70**, 260 (1999).
[31] R. Hawryluk, Proc. of Physics of Plasmas Close to Thermonuclear Conditions **1**, 19 (1979).
[32] R. E. Waltz *et al.*, Phys. Plasmas **4**, 2482 (1997).
[33] S. Inagaki *et al.*, Plasma Phys. Control. Fusion **48**, A251 (2006).
[34] C. Sung *et al.*, Phys. Plasmas **23**, 042303 (2016).
[35] O. Meneghini *et al.*, Nucl. Fusion **55**, 083008 (2015).